Project 019 Development of Aviation Air Quality Tools for Airshed-Specific Impact Assessment: Air Quality Modeling

University of North Carolina at Chapel Hill

Project Lead Investigator

Saravanan Arunachalam, PhD
Research Professor
Institute for the Environment
University of North Carolina at Chapel Hill
100 Europa Drive, Suite 490
Chapel Hill, NC 27517
919-966-2126
sarav@email.unc.edu

University Participants

University of North Carolina at Chapel Hill

- PI: Saravanan Arunachalam, Research Professor and Deputy Director
- FAA Award Number: 13-C-AJFE-UNC, Amendments 1–15
- Period of Performance: October 1, 2020 to September 30, 2021
- Task: Develop a framework for a new dispersion model for aircraft sources

Project Funding Level

FAA provided $569,000 in funding. Matching cost-sharing was provided by EU-AVIATOR and the Environmental Defense Fund.

Investigation Team

Prof. Saravanan Arunachalam (UNC) (PI) [Task 1]
Dr. Chowdhury Moniruzzaman (UNC) (Co-Investigator) [Task 1]
Dr. Gavendra Pandey (UNC) (Co-Investigator) [Task 1]
Mr. Brian Naess (UNC) (Co-Investigator) [Task 1]
Mr. Praful Dodda (UNC) (Graduate Research Assistant) [Task 1]
Prof. Akula Venkatram (University of California, Riverside) (Consultant) [Task 1]

Project Overview

Aviation is predicted to grow steadily in upcoming years;[1] thus, a variety of aviation environmental policies will be required to meet emission reduction goals in aviation-related air quality and health impacts. Tools are needed to rapidly assess the implications of alternative policies for an evolving population and atmosphere. In the context of the International Civil Aviation Organization (ICAO), Committee on Aviation Environmental Protection (CAEP), additional approaches are required to determine the implications of global aviation emissions.

The overall objective of this project is to develop a new aircraft-specific dispersion model and continue the development and implementation of tools, both domestically and internationally, to allow for an assessment of year-to-year changes in significant health outcomes. These tools must be acceptable to the FAA (in the context of Destination 2025) and/or other decision-makers. More importantly, this new model must have the capability to address the 1-hour form of the NO_2 National Ambient Air Quality Standard (NAAQS) in the United States (U.S.) and to support National Environmental Policy Act (NEPA)

[1] Boeing Commercial Airplane Market Analysis, 2010.

and/or NAAQS analyses that may be needed by airports. The developed methods must also rapidly provide output to support a variety of "what-if" analyses and other investigations. While the tools for use within and outside the United States need not be identical, a number of goals are desirable for both cases:

- Enable the assessment of premature mortality and morbidity risks due to aviation-attributable particulate matter (PM) with a diameter up to 2.5 μm ($PM_{2.5}$), ozone, and other pollutants known to exert significant health impacts;
- Capture airport-specific health impacts at regional and local scales;
- Account for the impact of landing/takeoff (LTO) versus non-LTO emissions, including a separation of effects;
- Allow for an assessment of a wide range of aircraft emission scenarios, including differential growth rates and emission indices;
- Account for changes in nonaviation emissions;
- Allow for assessments of sensitivity to meteorology;
- Provide domestic and global results;
- Include quantified uncertainties and differences with respect to Environmental Protection Agency (EPA) practices, which are to be minimized when scientifically appropriate; and
- Ensure computational efficiency such that tools can be used in time-sensitive rapid turnaround contexts and for uncertainty quantification.

During this period of performance, the (UNC) Institute for the Environment (UNC-IE) team performed work on a single task with four subtasks, as described below.

1. Develop a new dispersion model for aircraft sources with four subtasks:
    1. Source Characterization
    2. Physical Processes
    3. Chemical Processes
    4. Model Evaluation

Task 1 – Develop a Framework for a New Dispersion Model for Aircraft Sources

University of North Carolina at Chapel Hill

Objective(s)

The FAA's Aviation Environmental Design Tool (AEDT) is currently coupled with the U.S. EPA's AERMOD dispersion model for modeling aircraft sources and is the required regulatory model in the U.S. for modeling airport-level aircraft operations during LTO cycles.

Recent studies have shown several limitations in the use of AERMOD for modeling aircraft sources. In 2011, the Airport Modeling Advisory Committee (AMAC) developed a series of recommendations to improve jet exhaust modeling. Since then, Airport Cooperative Research Program (ACRP) project 02-08 has developed guidance for airport operators on conducting measurements and modeling for air quality at airports, published in ACRP Report 70 (Kim et al., 2012). This study conducted a measurement and modeling study at Washington Dulles International Airport (IAD). More recently, ACRP project 02-58 developed a final ACRP Report 171 (Arunachalam et al., 2017a) for providing dispersion modeling guidance for airport operators regarding local air quality and health. This study applied four dispersion models—AERMOD, CALPUFF, SCICHEM, and the U.K.'s ADMS-Airport—for the Los Angeles International Airport (LAX) and compared model predictions with high-resolution measurements taken during the Los Angeles Air Quality Source Apportionment Study (AQSAS). Each of these reports identified several limitations with AERMOD and developed a series of recommendations for improving dispersion modeling of aircraft emissions for airport-level air quality.

UNC recently developed the C-AIRPORT dispersion model for application to LAX (Arunachalam et al., 2017c). Initially, C-AIRPORT was designed to be part of the C-TOOLS series of community-scale, web-based modeling systems. The objective of C-TOOLS was to create a web-based interface to model multiple source types for short-term or long-term pollutant concentration averages and to perform various what-if scenarios that assess changes in air quality at local scales due to changes in inputs. C-AIRPORT uses a line-source-based approach to model aircraft sources, based upon the C-LINE modeling system (Barzyk et al., 2015), and a preliminary evaluation of the algorithms in comparison with LAX AQSAS was conducted.

Under the previous year's funding, UNC-IE developed a comprehensive plan for a modeling framework that addresses known limitations from the above Tasks and proposed a viable, more suitable approach for modeling pollutants from aircraft sources. The primary objective of this plan is to demonstrate that a robust, improved pollutant dispersion model for aircraft can be developed for U.S. regulatory compliance purposes. The proposed new model will disperse pollutants from aircraft sources in a more technically and scientifically advanced manner (compared with current AERMOD capabilities), with the ultimate goal of use as a potential U.S. regulatory compliance tool, based on ongoing discussions between the FAA and EPA. This plan will include an itemized list of known limitations along with a corresponding proposed developmental approach providing recommendations on how to address these limitations.

As part of this Task, we proposed implementing the plan with specific focus on four broad areas over a period of two years.

Our approach aims to ensure that the new model will be "robust" and based on the state of science on source and plume characterization and associated algorithms.

1) **Source Characterization**
   In this area, we explore alternate options beyond the current area-source-based approach in the AERMOD model. Some approaches we explored include:
   - Volume treatment in AERMOD,
   - Puff-based treatment, as in SCICHEM,
   - Line-based treatment, as in C-AIRPORT, and
   - Line-puff or jet sources, as in ADMS-Airport.
2) **Physical Process Assessment**
   In this area, we assess all relevant processes for aircraft dispersion, including the treatment of plume rises, wing tip vortices, and low-wind-speed conditions. Some specific approaches include:
   - A coupled plume rise-wake model for assessing the effects of wake vortices on plume rise, dispersion, and ground-level concentrations and
   - An integral approach called the fluid-mechanical entrainment model (FEM), which has been evaluated against light detection and ranging (LIDAR) observations from Heathrow Airport (see Arunachalam et al., 2017a).
3) **Chemical Process Assessment**
   We will go beyond the initial implementation from last year, with a specific focus on the following aspects:
   - Recognition that the 1-hr form of the NO_2 NAAQS is a critical issue for air quality around U.S. airports, with several modeling studies showing overestimates of these compared with observations; it is important that the new model performs adequately to capture this short-term form of the NO_2 NAAQS;
   - A new detailed chemical mechanism for NO_2 including the generic reaction set (GRS) mechanism (Venkatram et al., 1994; Valencia et al., 2017) or others; and
   - A condensed version of the aerosol treatment, as included in CMAQ and SCICHEM and described by Chowdhury et al. (2015).
4) **Model Evaluation**
   Ongoing model evaluation has involved evaluating model predictions using only measurements from the LAX AQSAS for 2012. We will now work to develop and test the model for other case studies, including the following:
   - One of three airports (Copenhagen, Madrid, and Zurich) with measurements being undertaken as part of the EU-AVIATOR project (see https://aviatorproject.eu/) and
   - The Long Island Sound Tropospheric Study (LISTOS) project-based high-resolution measurements of NO_2 (and other pollutants) around the John F. Kennedy (JFK) International Airport in New York City (see https://ui.adsabs.harvard.edu/abs/2018AGUFM.A34B..01M/abstract).

   Model evaluation will focus on the model's ability to capture the behavior of the plume related to aircraft sources during LTO cycles at an airport in comparison with available observations and identifying strengths and weaknesses compared with other existing models.

Research Approach

In this report, we describe progress made on the four subtasks. Results from Subtask 1d are embedded in the descriptions for Tasks 1a–1c.

1. Source Characterization

1.1 Emissions Processing of AEDT Emissions (AEDT2ADM)

A Python-based emission processor, named "AEDT2ADM", has been developed to produce emission files of both new ADM and AERMOD dispersion models using AEDT flight segment data. We have updated the emission processor and evaluated the flight segment data for both winter and summer 2012 AEDT files.

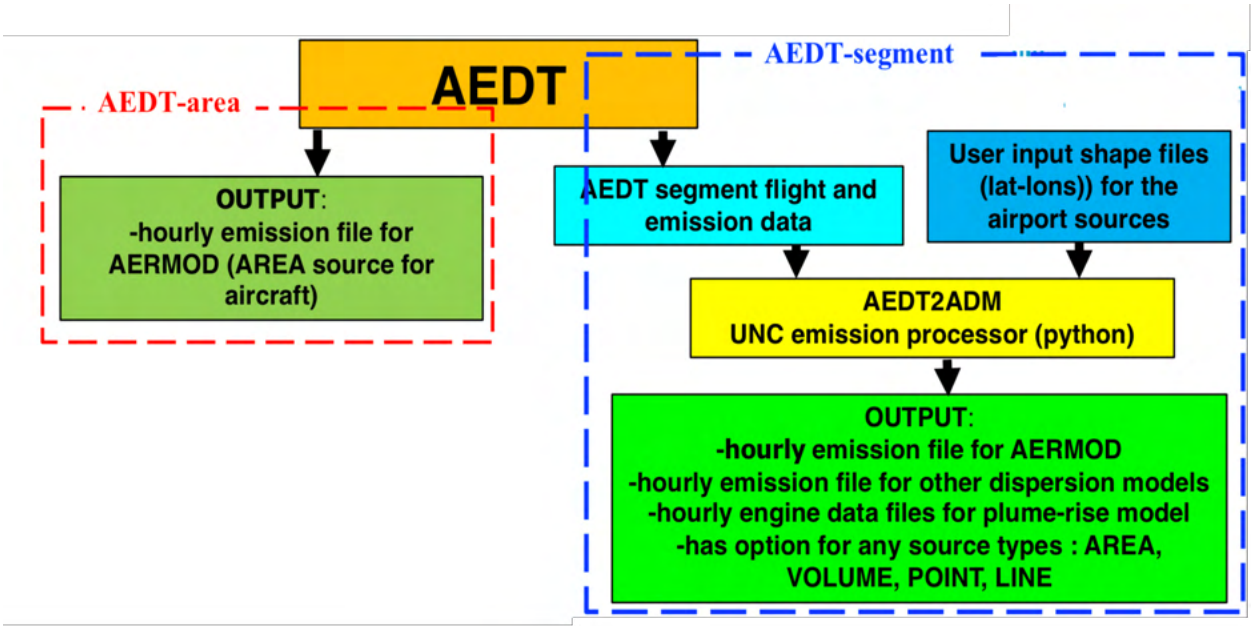

Figure 1.1. Schematic of the input/output data flow for the AEDT2ADM emission processor.

1.1.1 Update of the AEDT2ADM emission processor

The AEDT2ADM emission processor has been updated to include multiple new features since the last version reported in the UNC's ASCENT 2020 annual report. The new updates are described in section 1.1.1.1 to 1.1.1.5.

1.1.1.1 Added capability to produce emission files for all species for all dates in a single run

The 2020 version of the code was designed for only two species (NO_x and SO_x) and for only a single day. The code needed to run 29 times for 29 days to produce February 2012 data. The AEDT2ADM emission processor has been updated and can now produce emission files for all species present in the AEDT segment files for each day for an entire time period in a single run.

1.1.1.2 Added capability to produce ADM-formatted emission files

The AEDT2ADM emission processor has been updated to produce emission files in the desired format for ADM models.

1.1.1.3 Increase of spatial resolution of the surface source design

AEDT2ADM has been updated so that the user can provide source files (latitude and longitude of each area source) based on the user's source design. In this way, AEDT2ADM now has the capability to increase or decrease the spatial resolution of sources. The 138 surface sources in the latest version are shown in Figure 1.2, where sources are grouped in 5 categories shown in 5 colors.

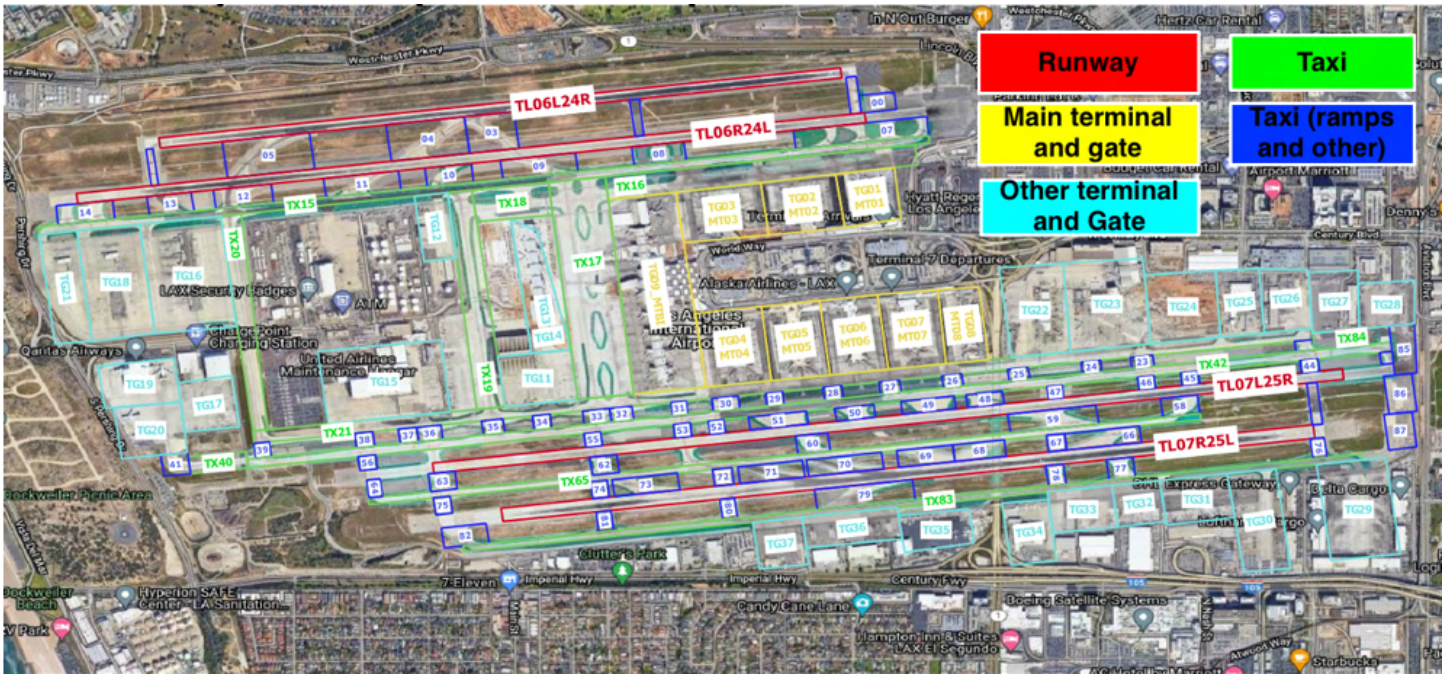

Figure 1.2. The 138 surface sources for LAX for the AEDT2ADM emission processor.

A sensitivity study was performed in which three sensitivity runs for the following three cases were performed by three AERMOD run cases:

- AEDT-area: 1440 area sources
- AEDT2ADM: 138 surface sources
- AEDT2ADM: 31 surface sources

A sensitivity study was performed to determine the model performance for these three source-number cases. The sensitivity results on the effect of a reduced number of surface sources on surface pollutant concentration in AERMOD dispersion modeling (Figure 1.3) showed that although the number of sources decreased from 1440 to 138 and to as few as 31, the diurnal profile showed little change from the results for the case of AEDT with 1440 surface sources.

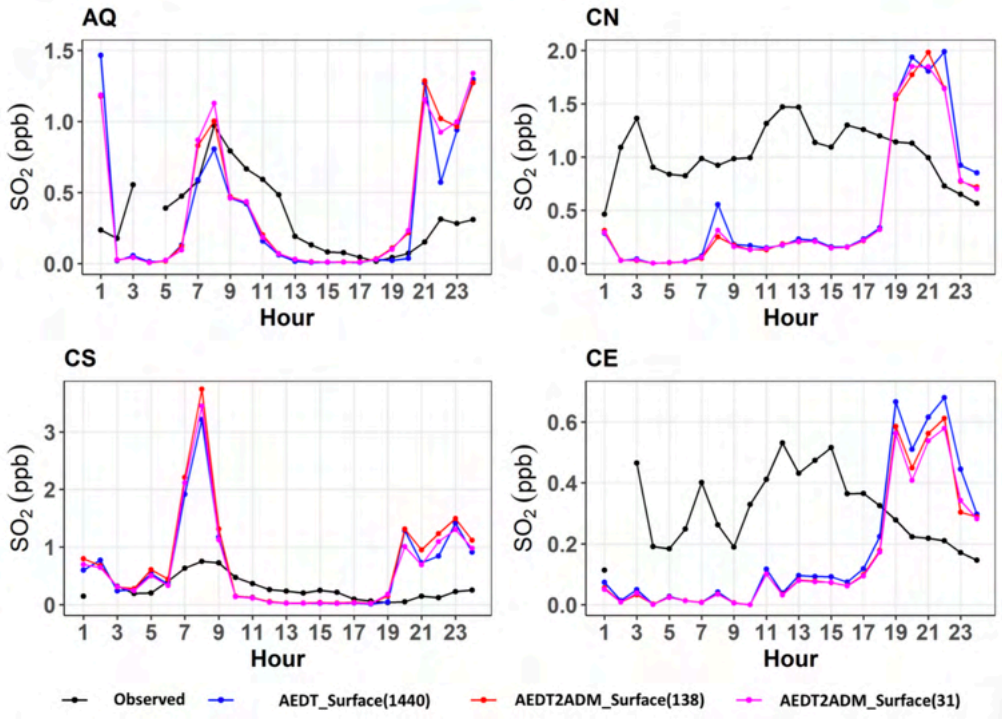

Figure 1.3. Diurnal profiles of SO_2 concentrations for one-month average data for each hour for three source-number cases: (1) AEDT 1440 surface sources (blue line), (2) AEDT2ADM 138 surface sources (red line), and (3) AEDT2ADM 31 surface sources for LAX in February 2012.

AERMOD modeling results for one month (February 2012) showed that a 90% surface source reduction (from 1440 to 138) decreased the computation time by 90% and increased the mean absolute error (MAE) by 3.5% and 12.3% at the AQ (Air Quality) and CS (Community South) sites and decreased the MAE by 2.8% and 4.8% at the CN (Community North) and CE (Community East) sites, respectively. A 98% reduction in surface sources (from 1440 to 31) decreased the computation time by 95% and increased the MAE by 3.9% and 1.2% at AQ and CS and decreased the MAE by 3.2% and 5.2% at CN and CE, respectively.

1.1.1.4 Added capability to produce emission files for AERMOD

The AEDT2ADM emission processor has been updated to produce emission files for AERMOD for user-provided surface source shape (latitude–longitude) files.

1.1.1.5 Added capability to produce aircraft-engine data files for the plume rise model for ADM

We updated the Python emission processor code AEDT2ADM and produced five ADM-formatted hourly average aircraft engine variables for the plume rise model. The five engine variables are:

- Fuel burn rate (segment number average fuel burn rate over one hour for a source),
- Thrust (fuel-burn-weighted average thrust for all segments over one hour for a source),
- Aircraft speed (segment number average aircraft speed over one hour for a source),
- Bypass ratio (average bypass ratios for all segments over one hour for a source) from AEDT data files, and
- Air–fuel ratio (average air–fuel ratios for all segments over one hour for a source) estimated for four LTO scenarios from a reference paper (Wayson et al., 2009).

The fuel burn rate, thrust, and aircraft speed for one source's data are shown in Table A1 in Appendix A for the plume rise model, whose values seem reasonable. The thrust (fuel-burn-rate-weighted average thrust for all segments over one hour for

a source) was compared with the segment number average thrust of a Boeing 737-300 aircraft engine from the AEDT-segment data file, as shown in Figure A1 in Appendix A, which shows hourly average thrust values within the normal range.

The newly developed plume rise model was applied to AEDT-segment data for different flights. We compared the average buoyancy for different segments for five different aircrafts with reported values for ADMS-Airport (https://www.cerc.co.uk/environmental- software/ADMS-Airport-model.html), as shown in Figure 1.4. The buoyancy was similar to results obtained by ADMS-Airport for B737 and B777, with an underprediction for B747 and an overprediction for A320 and A330, as shown in Figure 1.4. The buoyancy equation in the latest plume rise model successfully produced the buoyancy trend for aircraft engine size, where the largest engine (B777) has the highest buoyancy, which is consistent with the ADMS-Airport model results shown in Figure 1.4.

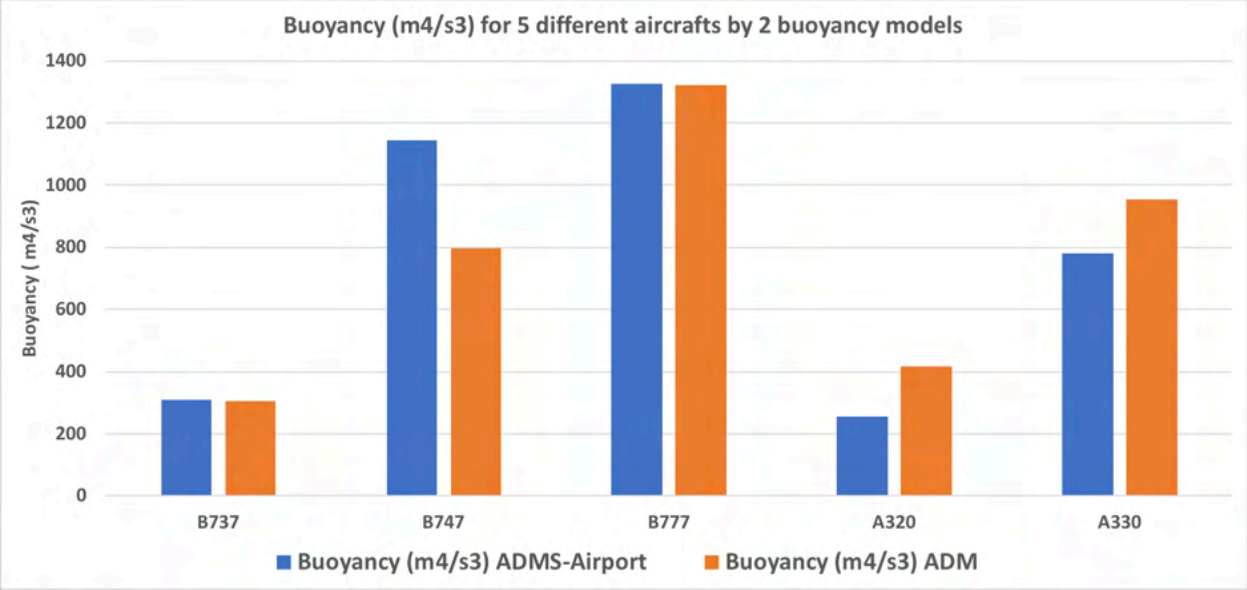

Figure 1.4. Comparison of buoyancy for the ADM with ADMS-Airport models (https://www.cerc.co.uk/environmental-software/ADMS-Airport-model.html) for five different aircraft.

1.1.2 Evaluation of winter and summer 2012 AEDT-segment data files

The values of variables in the summer and winter 2012 AEDT-segment files have been evaluated through a comparison with reference or typical values. Some findings are summarized in subsections 1.1.2.1–1.1.2.3.

1.1.2.1 Removal of zero-duration segments

The winter 2012 AEDT-segment data file has some rows with a zero value for "Duration." Analysis of the zero-duration segments provided the following findings:

- There are 1,815 zero-duration segments among 1,996,543 segments for 29 days in the February 2012 file, corresponding to 0.09%, as shown in Table A2 in Appendix A.
- In our initial postprocessing, we removed these 1,815 zero-duration ("00:00:00.00") segments from the main file and produced an emission inventory, which may have caused a 0.09% reduction in NO_x and SO_x emissions.
- Removing the 0.09% of segments may not cause any problems in the emission inventory.

1.1.2.2 Negative thrust

The winter and summer AEDT-segment data files have some rows with negative thrusts. A comprehensive analysis was performed on the negative thrust values and was described in a report to the FAA. Our findings were as follows:

- Approximately 1.7% of the segments in a 1.5-month winter file and 5.7% of segments in a 2-month summer file had negative thrusts for all altitudes, and approximately 1.4% and 2.3% of segments within LTO (3,000 ft) height had negative thrusts for one specific day in the winter and summer files, respectively, as shown in Table 1.1.
- The winter file had negative thrust values both at the surface and in air, but the summer file had negative thrust values only in air, as shown in Table A3 (can be seen in the minimum altitude for negative thrust segments in the winter and summer files).
- Analysis of the winter 2012 data file showed both civilian aircrafts and military aircrafts with negative thrusts.

Table 1.1. Number of segments with negative thrust values in winter and summer 2012 AEDT data files for LAX.

Files	Height	Total no of segments	No of negative thrust segments	% Negative thrust segments
Winter 2012 files				
1.5 months winter file	all height	3,603,655	62,155	1.72
1 day: Feb 1, 2012	all height	84,047	1,555	1.85
1 day: Feb 1, 2012	LTO height (<3000 ft)	62,485	898	1.44
Summer 2012 files				
2 months summer file	all height	5,983,658	315,176	5.27
1 day: July 1, 2012	all height	93,715	4,983	5.32
1 day: July 1, 2012	LTO height (<3000 ft)	64,573	1,531	2.37

1.1.2.3 Comparison of winter and summer 2012 AEDT-segment files

A comprehensive analysis has been performed to evaluate the winter and summer 2012 AEDT-segment files for LAX.

a. Comparison of non-emission parameters

We reviewed the FAA-AEDT summer file and compared it with the winter file, whose summary is given in Table A4 in Appendix A. The comparison shows that the AEDT-segment summer file has 126 variables whereas the winter file has 38. The summer file has 6 million rows for 2 months of data whereas the winter file has 3.7 million rows for 1.5 months of data. The summer file has two useful variables: (1) the number of engines per aircraft and the bypass ratio, which will be used to calculate air mass flow rate; and (2) the propulsion efficiency, which will be used in the plume rise model. The AEDT-area (AERMOD) summer file has three species (NO_x, SO_x, and CO), and the winter file has two species (NO_x and SOx). The AEDT-area (AERMOD) summer file has 21,660 sources whereas the winter file has 5,919 sources.

b. Comparison of emissions

The total emissions of all species have been compared between the winter and summer files. A summary of the comparison for SO_x and NO_x only is given in Tables A5 and A6 in Appendix A, respectively. The results of the comparison of other species can be shared with the FAA upon request. Some findings for SO_x and NO_x are as follows:

- **SO_x and NO_x emissions in winter and summer files**
  - The SO_x emission rate is approximately 27% lower for surface + air, 18% lower for surface only, and 35% lower for air only in the summer file than in the winter file, as shown in Table A5 in Appendix A.
  - The NO_x emission rate is approximately 40% lower (for surface + air, surface only, and air only) in the summer file than in the winter file, as shown in Table A6 in Appendix A.

- **Comparison of emission rates in winter and summer files with reference values**
  - The NO_x and SO_x emission rates for the winter file are consistent with the LAWA2013 report (Arunachalam et al., 2013) and Next-Gen JPDO report (CSSI, 2009), as shown in Tables A5 and A6 in Appendix A, respectively.
  - Instances in which both the NO_x and SO_x emission rates in the summer file are inconsistent with the LAWA2012 summer values are shown in Tables A5 and A6 in Appendix A, respectively.
- **Comparison of emissions below and above 3,000 ft**
  - SO_x emissions were 68% below 3,000 ft and 32% above 3,000 ft for both the winter and summer files, as shown in Table A5 in Appendix A.
  - NO_x emissions were 58% below 3,000 ft and 42% above 3,000 ft for both the winter and summer files, as shown in Table A6 in Appendix A.

1.2 Area-S vs. Area-A vs. Volume Characterization

In aircraft dispersion modeling, characterization of the aircraft sources presents a challenging problem. To address this issue, we performed a sensitivity analysis based on source treatments such as AREA and VOLUME in the AERMOD dispersion model. For this task, we used SO_2 aircraft emissions from AEDT-area (directly generated by AEDT) and AEDT-segment (generated from AEDT2ADM). Here, we modeled only the aircraft sources. AERMOD results from AREA and VOLUME sources were compared with each other and with observed concentrations reported in the LAWA study for February 2012. The simulated results are presented in the form of diurnal plots and quantile–quantile (Q-Q) plots with a fractional bias (FB) based on the robust highest concentration and factor of two (FAC2) for the observations. The following results were obtained using 1) AEDT-Area emissions, and 2) AEDT-Segment emissions.

1.2.1 AEDT-area emissions

- The diurnal concentration behaviors are similar for both source treatments (AREA and VOLUME) at all sites due to the large number of VOLUME sources (Figure 1.5 (a)).
- For VOLUME source treatment, the model's ability to predict low SO_2 concentrations improved slightly, approaching a one-to-one line at all sites except CN (Figure 1.5 (b)).
- FAC2 improved from 14%, 21%, and 22% to 20%, 55%, and 38% at the AQ, CS, and CE sites, respectively, under VOLUME source treatment (Figure 1.5 (b)).
- The FBs for both source treatments are comparable for all four core sites (Figure 1.5 (b)).

1.2.2 AEDT-segment emissions

- Significant changes were observed in diurnal concentration behavior at all sites, especially the CS site, under the AEDT-segment-based VOLUME source treatment. These differences are likely due to the lower number of volume sources (Figure 1.5).

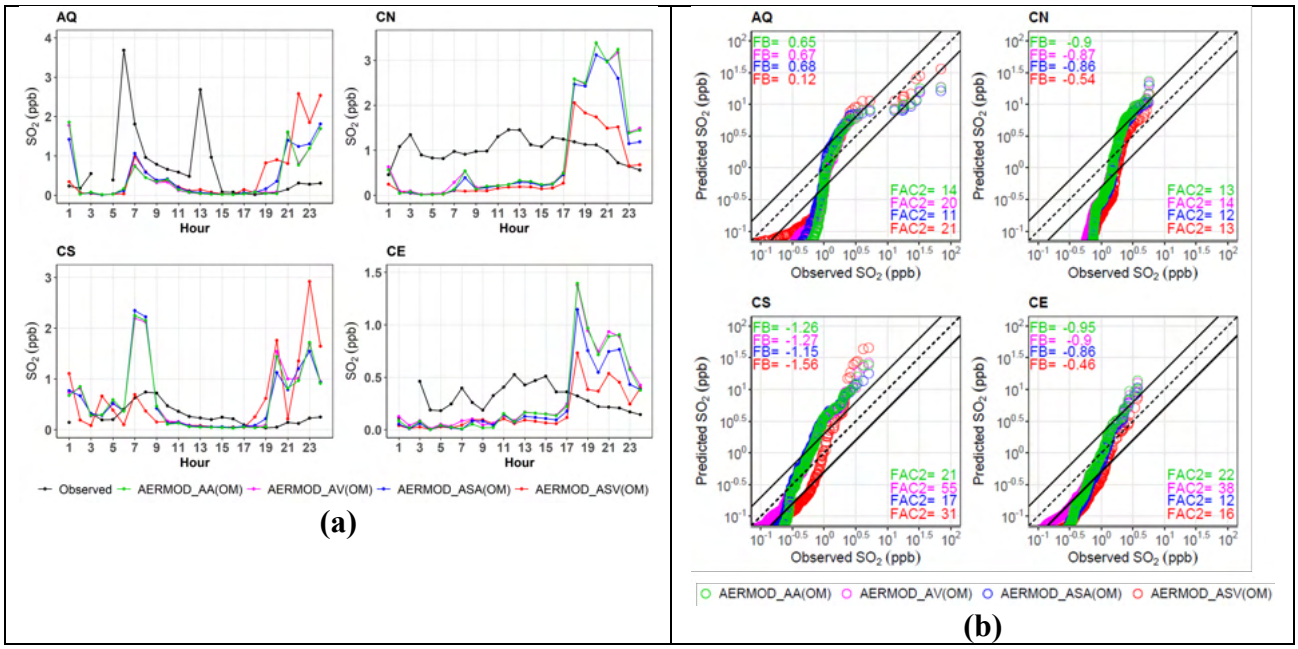

Figure 1.5 (a) Diurnal variability between observed and modeled SO_2 concentrations. **(b)** Q-Q plots for observed and predicted SO_2 concentrations for February 2012 at all four core sites (AQ, CN, CS, and CE). AA-AEDT: area-area source treatment; AV-AEDT: area-volume source treatment; ASA-AEDT: segment-area source treatment; ASV-AEDT: segment-volume source treatment; OM: original meteorology.

In addition, we conducted a sensitivity analysis based on the number of runway sources in AEDT-segment emissions. Here, we have depicted only the diurnal behavior of SO_2 predictions at the CS site (Figure 1.6). We found that as we increase the number of volume sources from 15 to 128, the results from VOLUME source treatment capture the characteristic patterns of diurnal concentrations obtained via AREA source treatment (Figure 1.6). Hence, the use of a larger number of volume sources enhances accuracy, and the results are comparable to those obtained from area sources.

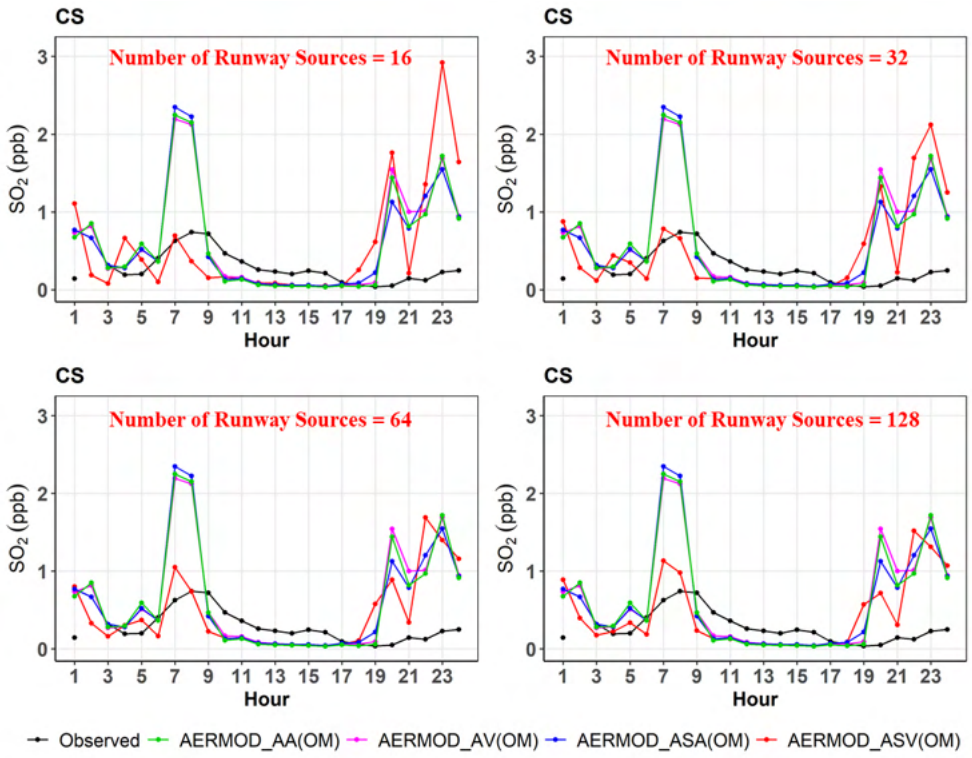

Figure 1.6. Diurnal variability between observed and modeled SO_2 concentrations for February 2012 at all four core sites (AQ, CN, CS, and CE). The notations are the same as those in Figure 1.5.

2. Physical Process Assessment

2.1 Plume Rise Treatment

In view of the incompleteness of the dispersion models used in aircraft dispersion modeling, we have developed a plume rise algorithm that builds upon our current understanding of the plume rise of emissions from stationary point sources.

The buoyancy parameter, F_b, that governs the plume rise from a point source is associated with energy output from an aircraft engine. The buoyancy parameter, F_b, of the exhaust plume is given by the following expression (Briggs, 1965):

$$F_b = \frac{g}{T_a} v_e r_0^2 \left(T_e - T_a\right), \quad (1)$$

where v_e and T_e are the velocity and temperature of the exhaust plume, T_a is the ambient temperature, and g is the acceleration due to gravity. The plume rise, h_{pb}, associated with a buoyant release from a point source in a neutral atmosphere is given by (Briggs, 1965):

$$h_{pb} = \left(\left(\frac{r_0}{\beta} \right)^3 + \frac{3}{2\beta^2} \frac{F_b}{U_{eff}^3} x^2 \right)^{1/3} - \left(\frac{r_0}{\beta} \right), \quad (2)$$

where $\beta = 0.6$ is an entrainment constant, x is the effective distance between the source and receptor, U_{eff} is the effective velocity within the plume, and r_0 is the initial radius of the plume. The final plume rise is calculated with the aid of two main plume rise parameters, such as buoyancy and momentum-induced plumes.

2.1.1 Computation of the buoyancy parameter from engine characteristics

Equation (1) for the buoyancy parameter can be written in terms of Q_e, the thermal power added to the air passing through the engine:

$$F_b = \frac{g}{T_a}\frac{Q_e}{\pi\rho_e C_p}, \quad (3)$$

where ρ_e is the exhaust density and C_p is the specific heat of the exhaust gas, which is mostly air.

After applying an energy balance for Q_e and performing further calculations for the thermal efficiency (η_t), we obtain the final buoyancy parameter term as:

$$F_b = \frac{g}{T_a}\frac{\dot{m}_f H_f \left(1-\eta_t\right)}{\pi\rho_e C_p}, \quad (4)$$

where the exit density, ρ_e, is computed from the energy conservation equation and the equation of state:

$$T_e = T_a + \frac{Q_e}{\dot{m}C_p}$$

$$\rho_e = \frac{p_a}{R_a T_e}. \quad (5)$$

Here, T_e is the average temperature of the exhaust gases, p_a is the ambient pressure, and R_a is the gas constant of air. We see that the inputs required to compute F_b are the thrust T, aircraft velocity v_a, fuel burn rate $\dot{m}_f$, air–fuel ratio AF, and engine bypass ratio, $bypr$.

2.1.2 Computation of jet momentum term

We assume that the horizontal momentum is conserved as the radius of the horizontal plume grows with distance from a stationary point within the area source. For a top-hat profile of velocity within the plume, the momentum balance can be written as:

$$\rho_p U_p \left(U_p - U_a\right)\pi r^2 = T, \quad (6)$$

where U_p is the velocity inside the plume relative to a stationary observer, U_a is the ambient velocity at the level of the plume, and ρ_p is the plume density. The initial momentum flow inside the plume is the thrust, T, exerted by the engine on the air. A version of this equation is derived in the appendix of Arunachalam et al. (2017).

As in Barrett et al. (2013), we assume that the radius of the jet exhaust grows linearly with distance from a point within the area source:

$$r = \alpha x + r_0, \quad (7)$$

where α is an entrainment constant and r_0 is the radius of the engine exhaust. The radius of the momentum plume is taken to grow until the difference between the plume and ambient velocities is comparable to the standard deviation of the ambient horizontal velocity fluctuation, $\sigma_u = 2.0u_*$, where u_* is the surface friction velocity. Then, the maximum plume radius is given by the following relationship:

$$T = \pi\rho_a r_m^2 \left(U_a + \sigma_u\right)\sigma_u, \quad (8)$$

where U_a is evaluated at $z = r_m$ and ρ_a is the ambient density. Then, r_m is given by:

$$r_m = \left(\frac{T}{\pi\rho_a (U_a + \sigma_u)\sigma_u}\right)^{1/2}. \quad (9)$$

The plume rise associated with momentum, h_{pm}, is taken to be the radius of the plume:

$$h_{pm} = r_0 + \alpha x \quad x \le x_m$$
$$= r_m \qquad x > x_m \,, \tag{10}$$

where x_m is the distance at which the radius reaches its maximum value:

$$x_m = \frac{(r_m - r_0)}{\alpha} \,. \tag{11}$$

The effect of buoyancy is considered by assuming that the buoyancy acts independently on the expanding jet plume.

We estimate the plume rise associated with buoyancy by applying a formulation applicable to point releases in a neutral atmosphere (Briggs, 1965):

$$h_{pb} = \left(\left(\frac{R}{\beta} \right)^3 + \frac{3}{2\beta^2} \frac{F_b}{U_{eff}^3} x^2 \right)^{1/3} - \left(\frac{R}{\beta} \right) \,, \tag{12}$$

where $\beta = 0.6$ is an entrainment constant, x is the effective distance between the area source and receptor, and U_{eff} is the effective velocity, which is taken to be the maximum of the velocity in the jet and the ambient velocity at plume height.

The buoyant plume rise interacts with that associated with horizontal momentum through the initial radius, R, in Equation (12). It is taken to be the average value of the radius of the momentum plume between 0 and x to account for the impact of momentum on the initial radius of the buoyant plume:

$$R = \frac{1}{x} \int_0^x r(x) dx \,, \tag{13}$$

which yields

$$R = r_0 + \alpha x / 2 \qquad x \le x_m$$
$$R = \frac{x_m}{x} \left(r_0 + \frac{\alpha x_m}{2} \right) + r_m \left(1 - \frac{x_m}{x} \right) \qquad x > x_m \,. \tag{14}$$

The buoyancy parameter, F_b, is computed from the equations described above. Equation (12) must be solved iteratively because the wind speed at the plume height is not known a priori.

The total plume rise is then:

$$h_p = h_{pb} + h_{pm} \,, \tag{15}$$

where the second term on the right-hand side is the plume rise associated with the momentum jet, given by Equation (10).

From Figure 2.1, we can clearly see how the plume rise varies with downwind distance for takeoff and landing for an individual area source. The maximum plume rise reaches 70 m for takeoff, whereas it reaches approximately 45 m for landing.

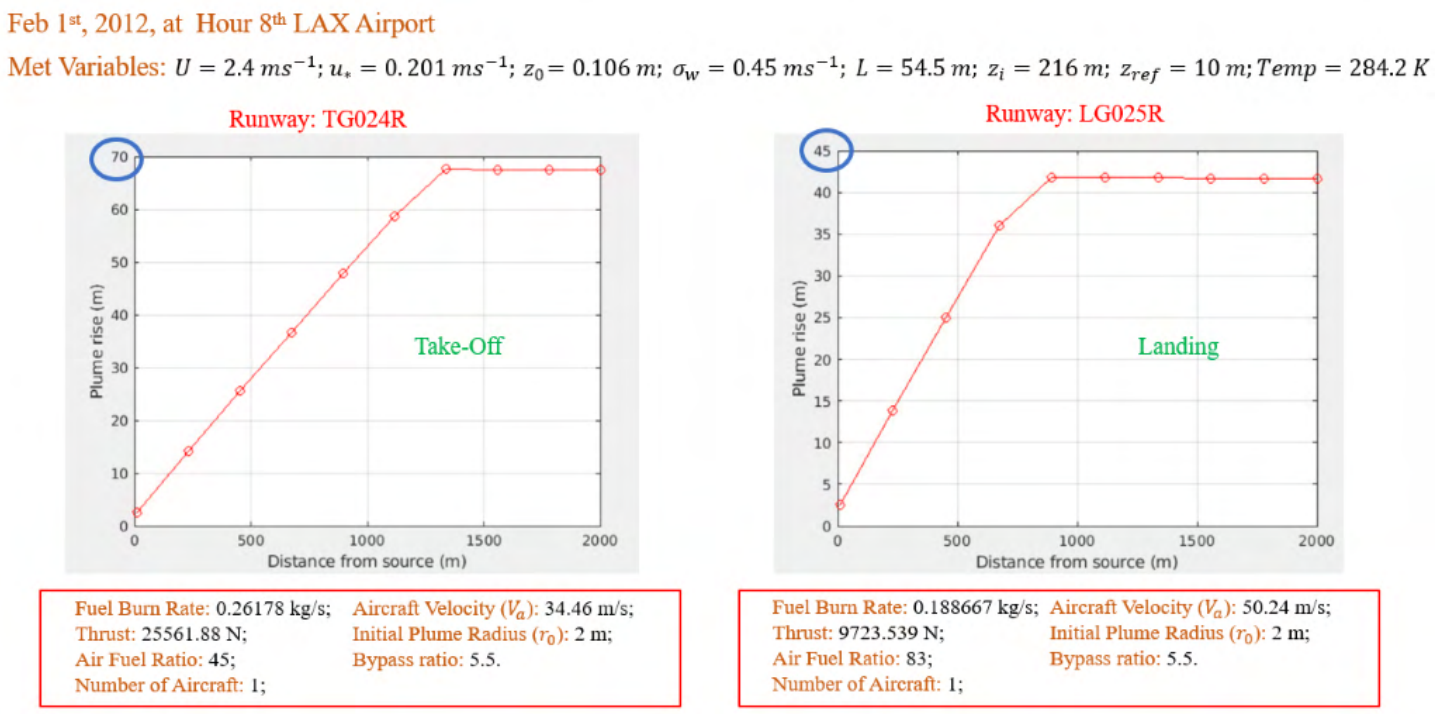

Figure 2.1. Plume rise for a single source at one hour for take-off and landing at LAX.

2.2 Alternate Treatment of Meteorological Inputs

Air quality assessments in and around an airport become more difficult when the airport is located near a shoreline or coastal region, where meteorological conditions are far from spatially uniform. In these conditions, the airport region never become highly unstable or highly stable due to the cold breeze from the ocean. The input preprocessor (AERMET) of AERMOD does not account for important features of the boundary layer present on the shoreline. We have modified the meteorological outputs from AERMET to account for the formation of an internal boundary layer when stable air from the ocean flows onto the warmer land surface of the airport. The sensitivity analysis led to the following changes:

- To account for the shoreline effect at LAX, stable and convective conditions in the AERMET file were replaced by neutral conditions: the Monin–Obukhov length was set to 1000 m, and the friction velocity was computed using the neutral formulation:

$$u_* = k\frac{U_r}{ln\left(\frac{z_r}{z_0}\right)}, \qquad (16)$$

  where k is the von-Karman constant, U_r is the wind speed at z_r (reference height), and z_0 is the roughness length.
- The roughness lengths (z_0) changed when the winds blew from the northeast quadrant to reflect flow passing over the Los Angeles urban core with tall buildings.

Here, the set of AERMET output parameters based on the above modifications is termed the modified meteorology (MM), whereas the AERMET-generated meteorological output is called the original meteorology (OM). For this analysis, we used SO_2 concentration measurements from the LAX AQSAS obtained for four core locations (AQ, CN, CS, and CE) for a 42-day period during February and March 2012, accounting for all airport and non-airport source emissions from the EDMS inventory (Arunachalam et al., 2017; ACRP Report 179).

In addition to applying the above meteorological inputs, we performed a sensitivity analysis based on sub-hourly treatment of the meteorological inputs.

2.3 Sub-hourly Treatment of Meteorological Inputs (SHARP)

Aircraft sources emit pollutants in short bursts, especially during LTO operations. It is difficult to quantify these short bursts of emissions and model the governing processes. Additional complexity arises when the wind speed is low and variable. In these conditions, winds can blow to/from several directions within a duration of one hour, resulting in multiple concentration "lobes" and large plume spread. Classical steady-state models such as AERMOD do not account for the meandering effect and short bursts of aircraft emissions resulting in hourly variations of inputs and outputs in typical applications. To account for these features characterizing the dispersion of aircraft emissions, a sensitivity analysis based on a sub-hourly approach is described here. To create meteorological inputs for these sub-hourly time scales, we used AERMINUTEplus (developed by AECOM), an enhanced version of the AERMET preprocessor AERMINUTE that outputs sub-hourly wind averages based on 1-minute ASOS data. The output from AERMINUTEplus is used in AERMET, AERMOD is run multiple times for each portion of an hour, and then output concentration files are simply averaged for that hour using a previously developed approach called the Sub-Hourly AERMOD Run Procedure (SHARP) (Figure 2.2).

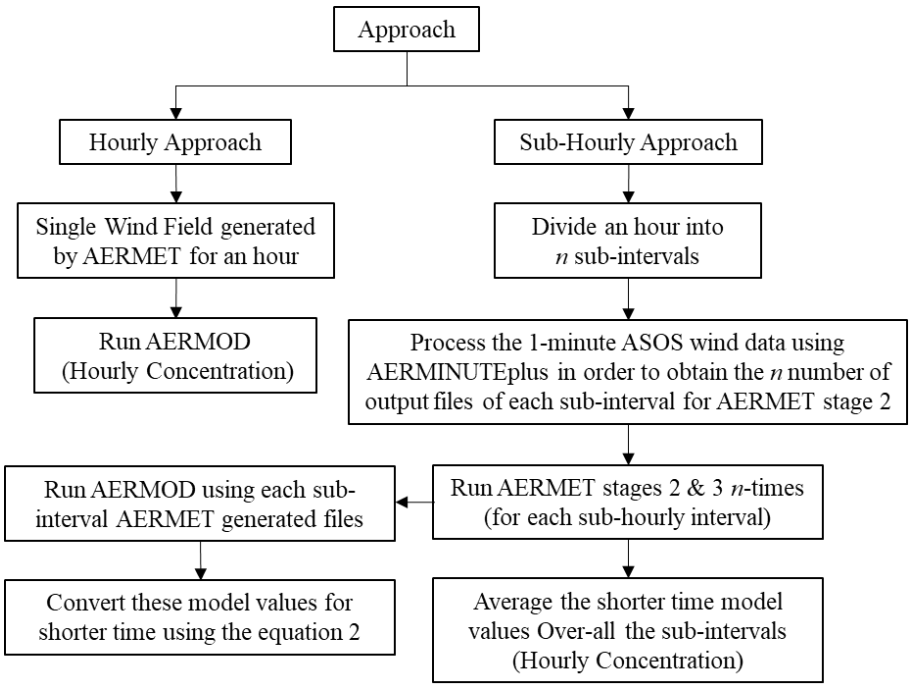

Figure 2.2. Hourly and sub-hourly calculations.

The diurnal concentration peaks decrease with the sub-hourly approach, particularly for the CS site (Figure 2.3(a)). In addition, the sub-hourly approach with MM showed a greater improvement in the results and largely captured most of the high peaks at all sites (Figure 2.3(a)). Hourly AERMOD simulations produced concentrations that were significantly greater than those at AQ and CS and significantly lower than those at CN and CE in the Q-Q distribution (Figure 2.3 (b)). The FB based on the top 26 robust highest concentrations increased from -1.50 and -1.37 to -0.91 and -0.79 at sites AQ and CN with the sub-hourly approach, whereas with MM, these values are improved as -0.05 and 0.15 respectively at sites AQ and CN. However, these approaches showed little change at sites CS and CE (Figure 2.3(b)). The use of the SHARP approach with MM magnifies the mid- to lower-range concentrations, and the lower concentrations nearly match the observations. The fraction of model estimates within a factor of two of the observations increased from 32% to 47% at the CN site and by up to 46% at the CS site (Figure 2.3(b)). Overall, our sub-hourly modeling results using SHARP and MM are relatively closer to the observations and demonstrate that this alternate approach should be seriously explored in circumstances when low-wind meander conditions predominate for modeling aircraft sources.

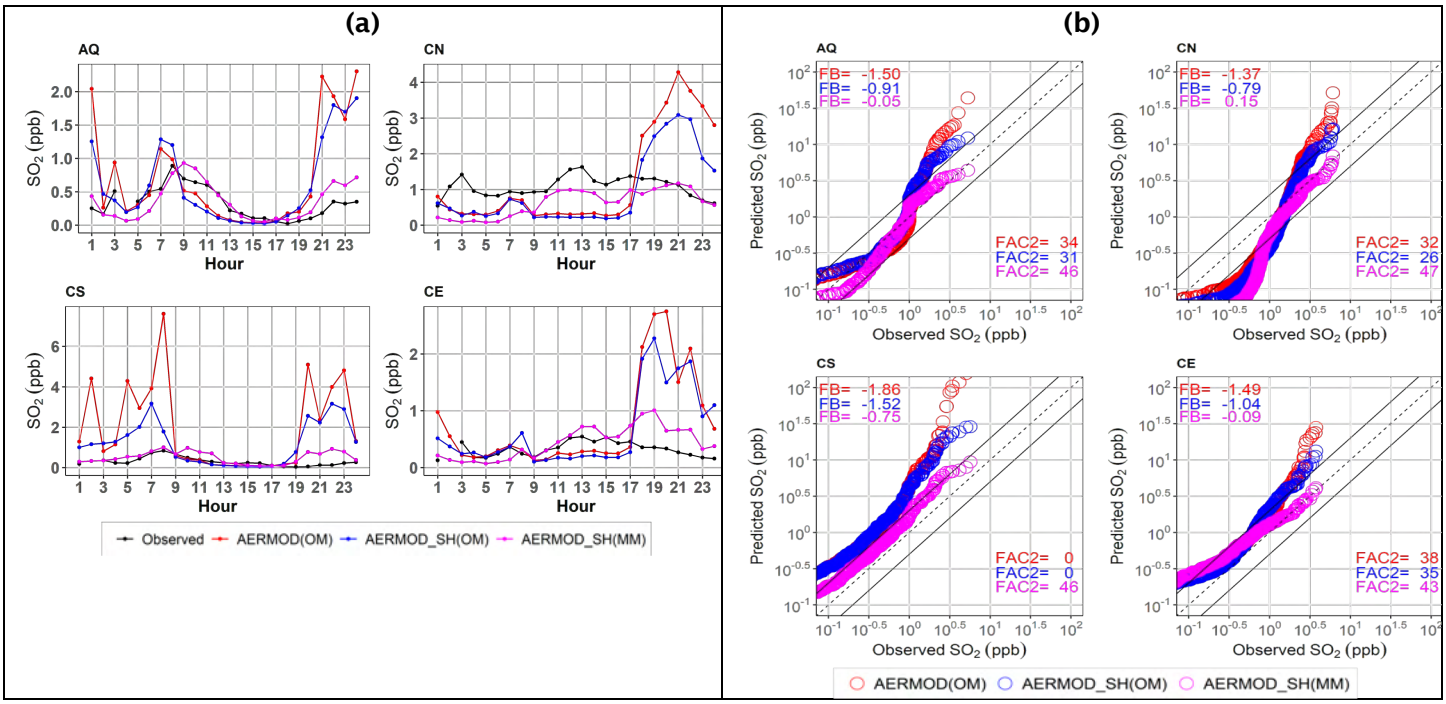

Figure 2.3. (a) Diurnal variability between observed and modeled SO_2 concentrations. **(b)** Q-Q plots for observed to predicted SO_2 concentrations for winter 2012 (42 days) at all four core sites (AQ, CN, CS, and CE). SH: sub-hourly area source treatment; OM: original meteorology; MM: modified meteorology.

3. Chemical Process Assessment

3.1 Gas-phase Treatment

Different reaction mechanisms have been reviewed for the chemistry module for the ADM. One reaction mechanism named Generic Reaction Set (GRS) mechanism (Azzi et al., 1992), as shown in Table B1 in Appendix B, was chosen for the initial tests. The second reaction mechanism (Venkatram et al., 1997), shown in Figure B1 in Appendix B, has a higher number reactions with an empirical aerosol formation reaction, which is modified from the GRS mechanism (Azzi et al., 1992) and is denoted hereafter as the MGRS mechanism. Box model simulations were performed for these two reaction mechanisms for initial tests.

3.1.1 Box model simulation of the GRS mechanism by rate constant for three different reference sources

Box model simulations were performed for the GRS mechanism using the rate constants shown in Figure B2 in Appendix B, which were obtained from three papers: (1) GRS mechanism, Azzi et al., (1992), (2) Valencia et al. (2018), and (3) Pournazeri et al. (2014), as shown in Table B1 in Appendix B. Few reactions are different among the three papers shown in Table B1 in Appendix B. The rate constants from Valencia et al. (2018) give the best results in comparison with the observations shown in Figure B2 in Appendix B. Both NO and O_3 results from box models for the three reaction rate cases follow the trend and magnitude of the observation (right figure) shown in Figure B2 in Appendix B. The reaction rate for the GRS mechanism (Valencia et al., 2018) can be used for the chemistry module of the ADM.

3.1.2 Determination of the reactive organic carbon/volatile organic compound (ROC/VOC) ratio

The lumped hydrocarbon VOC species may not be as reactive as individual real reactive organic carbon (ROC) species (Venkatram et al., 1994). Hence, ROC estimations from VOC were proposed by Venkatram et al. (1994). The ROC/VOC ratio has been estimated based on Venkatram et al. (1994). The ROC emission rate was estimated through the following steps:

- The mole fraction, molecular formula, and molecular weight of VOCs were estimated based on the speciation of VOCs from Wilkerson et al. (2010) and the VOC definition from the FAA-EPA Report (EPA, 2009), as shown in Table 3.1.

- The following were calculated based on the nine lumped VOC species and their reactivity from Venkatram et al. (1994):
    - The mass ratio of ROC/VOC in emissions must be 14.11 (ROC emission in the GRS model must be 14.11 times the VOC emission).
    - The molar ratio of ROC/VOC in emissions must be 17.30.
    - The VOC average molecular formula is $C_{3.2}H_6O_{0.43}$.
    - The VOC average molecular weight is 51.38.

Table 3.1 Estimating the ROC emission rate (ROC/VOC mass ratio) based on the reactivity of eight lumped VOC species (Venkatram et al., 1994) and speciated VOCs from Wilkerson et al. (2010) and the average elemental composition of VOCs.

VOC	Reactivity (RA)	ADOM VOC Species	Mass Fraction (MSF)	Mole fraction (MLF)	ROC/VOC Ratio MSF*RA	ROC/VOC Ratio MLF*RA	Average Molecular Formula	Average Molecular Weight
Propane, benzene	0.170	C3H8	0.023	0.012	0.004	0.002	C5.77H6.15	
Higher alkane (C>4)	0.430	ALKA	0.177	0.063	0.076	0.027	C10.17H22.33	
Ethylene	10.370	ETHE	0.239	0.420	2.482	4.354	C2.13H3.89	
Higher alkene, biogenics (C>2)	24.970	ALKE	0.135	0.082	3.363	2.039	C6.12H11.85	
Mono-alkyl-benzenes	8.760	TOLU	0.009	0.005	0.078	0.042	C7.30H8.61	
Di- and tri-alkyl-benzenes	24.850	AROM	0.038	0.016	0.948	0.396	C9.40H11.06	
Formaldehyde	42.170	HCHO	0.123	0.213	5.190	8.964	C1H2O1	
Higher aldehyde	6.700	ALD2	0.190	0.136	1.271	0.912	C4.025H7.851	
Ketones	10.490	MEK	0.067	0.054	0.700	0.563	C2.77H3.54O1.50	
Sum Total (VOC)			**1.000**	**1.000**	**14.112**	**17.299**	**C3.20H6.00O0.43**	**51.38**

3.1.3 Output of ROC emission files for February 2012 using the AEDT VOC emission files

ROC emission files were produced for February 2012 by using the VOC emission rate from the AEDT2ADM emission processor and the estimated ROC/VOC ratio, which will be used in the GRS chemistry mechanism in the chemistry module of the ADM.

3.2 Aerosol-phase Treatment

Currently, we are planning to use the empirical aerosol formation reaction from the MGRS reaction mechanism (Venkatram et al., 1994) shown in Figure B1b, reaction 2, 3, 9, 10, 11, and 12. The rate constants of these new reactions in the MGRS

mechanism will be determined by box model simulations compared with box model measurements in which aerosol is produced and measured.

Milestone(s)

We submitted drafts of the following documents to the FAA:

- A design document for the ADM,
- Version 1 of the ADM, and
- A white paper on plume rise treatment.

Major Accomplishments

- Updated a design document detailing the features that will be included in the new ADM
- Developed a white paper on plume rise treatment with a focus on AERMOD
- Developed an initial version of plume rise treatment
- Drafted a paper on improved meteorology and evaluation at LAX AQSAS
- Completed initial work on creating sub-hourly meteorological inputs for AERMOD and evaluated the results against LAX AQSAS data

Publications

- Arter, C. A., Buonocore, J. J., Moniruzzaman, C., Yang, D., Jiaoyan, J., & Arunachalam, S. (2022). Air quality and health-related impacts of traditional and alternate jet fuels from airport aircraft operations in the U.S. Environment International, *158*, 106958. https://doi.org/10.1016/j.envint.2021.106958
- Arter, C. A., & Arunachalam, S. (2021). Assessing the importance of nonlinearity for aircraft emissions' impact on O_3 and $PM_{2.5}$. Science Of the Total Environment, *777*, 1462021. https://doi.org/10.1016/j.scitotenv.2021.146121
- Moniruzzaman, C. G., Bowden, J., & Arunachalam, S. (2020). Aircraft landing and takeoff emission impacts on surface O_3 and $PM_{2.5}$ through aerosol direct feedback effects estimated by the coupled WRF-CMAQ model. Atmosoheric Environment, *243*, 117859. https://doi.org/10.1016/j.atmosenv.2020.117859
- Pandey, G., Moniruzzaman, C., Venkatram, A., & Arunachalam, S. (2021, October 18-22). Effect of atmospheric stability on modeling air quality in and around a major airport [Presentation]. International Technical Meeting on Air Pollution Modeling and Its Applications (ITM), Barcelona, Spain.

Outreach Efforts

- Presentation at semi-annual ASCENT stakeholder meetings in the spring and fall of 2021, held virtually
- Presentation and collaborative discussion during monthly meetings with the FAA and EPA
- Presentation at monthly and annual AEC Roadmap meetings hosted by the FAA

Awards

None

Student Involvement

Mr. Praful Dodda contributed to Task 1.

Plans for Next Period

Finalize the ADM with all physical and chemical processes and perform a complete evaluation

References

Arunachalam, S., Blanchard, C., Henry, R., & Tombach, I. (2013). *LAX Air Quality and Source Apportionment Study Volume 1: Executive Summary.* Los Angeles World Airports. Retrieved from https://www.lawa.org/lawa-environment/lax/lax-air-quality-and-source-apportionment-study/final-report-and-materials

Arunachalam, S., Valencia, A., Woody, M., Snyder, M., Huang, J., Weil, J., Soucacos, P., & Webb, S. (2017). Dispersion modeling guidance for airports addressing local air quality concerns, Appendix G (Report No. 179). Transportation Research Board Airport Cooperative Research Program (ACRP), Washington, DC. http://nap.edu/24881

Azzi, M., Johnson, G. M., & Cope, M. (1992, July 5-10). An Introduction to the generic reaction set photochemical smog mechanism In: CSIRO Division of Coal and Energy Technology, North Ryde (Ed.) 11th International Conference of the Clean Air Society of Australia and New Zealand. Brisbane, Australia, 451–462.

Barrett, S. R. H., Britter, R. E., Waitz, I. A. (2013). Impact of aircraft plume dynamics on airport local air quality. Atmospheric

Environment, *74*, 247–258. https://doi.org/10.1016/j.atmosenv.2013.03.061

Briggs, G. A. (1965). A plume rise model compared with observations. Journal of the Air Pollution Control Association, *15*, 433–438. https://doi.org/10.1080/00022470.1965.10468404

CSSI, 2009, JPDO-NextGen-TDM23: Investigation of Aviation for Future Aviation Activity Scenario, Washington, DC.

Federal Aviation Administration, & U.S. Environmental Protection Agency. (2009), Recommended best practice for quantifying speciated organic gas emissions from aircraft equipped with turbofan, turbojet, and turboprop engines – Version 1.0. Federal Aviation Administration Office of Environment and Energy and U.S. Environmental Protection Agency Office of Transportation and Air Quality. https://www.faa.gov/regulations_policies/policy_guidance/envir_policy/media/FAA-EPA_RBP_Speciated%20OG_Aircraft_052709.pdf

Pournazeri, S., Tan, S., Schulte, N., Jing, Q., Venkatram, A. (2014). A computationally efficient model for estimating background concentrations of NO_x, NO_2, and O_3. Environmental Modelling & Software, *52*, 19–37. https://doi.org/10.1016/j.envsoft.2013.10.018

Valencia, A., Arunachalam, S., Heist, D., Carruthers, D., & Venkatram, A. (2018). Development and evaluation of the R-LINE model algorithms to account for chemical transformation in the near-road environment. Transportation Research Part D: Transport & Environment, 59, 464 – 477. https://doi.org/10.1016/J.TRD.2018.01.028

Venkatram, A., Karamchandani, P., Pai, P., & Goldstein, R. (1994). The development and application of a simplified ozone modeling system (SOMS). Atmospheric Environment, *28*, 3665–3678. https://doi.org/10.1016/1352-2310(94)00190-V

Venkatram, A., Karamchandani, P., Pai, P., Sloane, C., Saxena, P., & Goldstein, R. (1997). The development of a model to examine source-receptor relationships for visibility on the colorado plateau. Journal of the Air & Waste Management Association, *47*, 286–301. https://doi.org/10.1080/10473289.1997.10464453

Wayson, R. L., Fleming, G. G. & Iovinelli, R. (2009). Methodology to estimate particulate matter emissions from certified commercial aircraft engines. Journal of the Air & Waste Management Association *59*(1), 91-100. https://doi.org10.3155/1047-3289.59.1.91

Appendix A: Emission Processing

Table A1. Hourly average aircraft engine data (fuel burn rate, thrust, aircraft speed, bypass ratio [BPR], and air-fuel ratio [AFR]) for runway 24L takeoff produced by the emission processor code AEDT2ADM (all data for runway sources have been produced and saved in the ADM format; only one source is shown here).

Time	24L-Take-Off_Fuel_Burn (kg/s)	24L-Take-Off_Thrust (kN)	24L-Take-Off_Aircraft_Speed (m/s)	24L-Take-Off_BPR	24L-Take-Off_AFR
2/1/12 0:00	1.28	124.10	37.29	5.5	45
2/1/12 1:00	1.21	102.53	35.72	5.5	45
2/1/12 2:00	1.58	88.79	33.87	5.5	45
2/1/12 3:00	1.29	94.63	32.23	5.5	45
2/1/12 4:00	1.36	98.85	33.90	5.5	45
2/1/12 5:00	1.53	146.79	35.70	5.5	45
2/1/12 6:00	0.94	110.23	34.79	5.5	45
2/1/12 7:00	1.72	266.78	38.48	5.5	45
2/1/12 8:00	1.06	127.00	34.47	5.5	45
2/1/12 9:00	0.73	99.18	33.05	5.5	45
2/1/12 10:00	1.59	239.19	37.50	5.5	45
2/1/12 11:00	1.53	152.05	36.01	5.5	45
2/1/12 12:00	1.50	148.65	34.20	5.5	45
2/1/12 13:00	1.50	150.24	33.19	5.5	45
2/1/12 14:00	1.00	96.23	30.32	5.5	45
2/1/12 15:00	0.58	67.49	30.11	5.5	45
2/1/12 16:00	1.44	153.81	31.77	5.5	45
2/1/12 17:00	1.21	157.33	33.16	5.5	45
2/1/12 18:00	1.46	212.36	34.58	5.5	45
2/1/12 19:00	1.31	147.13	32.59	5.5	45
2/1/12 20:00	1.32	136.42	32.99	5.5	45
2/1/12 21:00	1.97	178.12	37.93	5.5	45
2/1/12 22:00	1.89	233.65	36.33	5.5	45
2/1/12 23:00	1.54	97.43	36.42	5.5	45

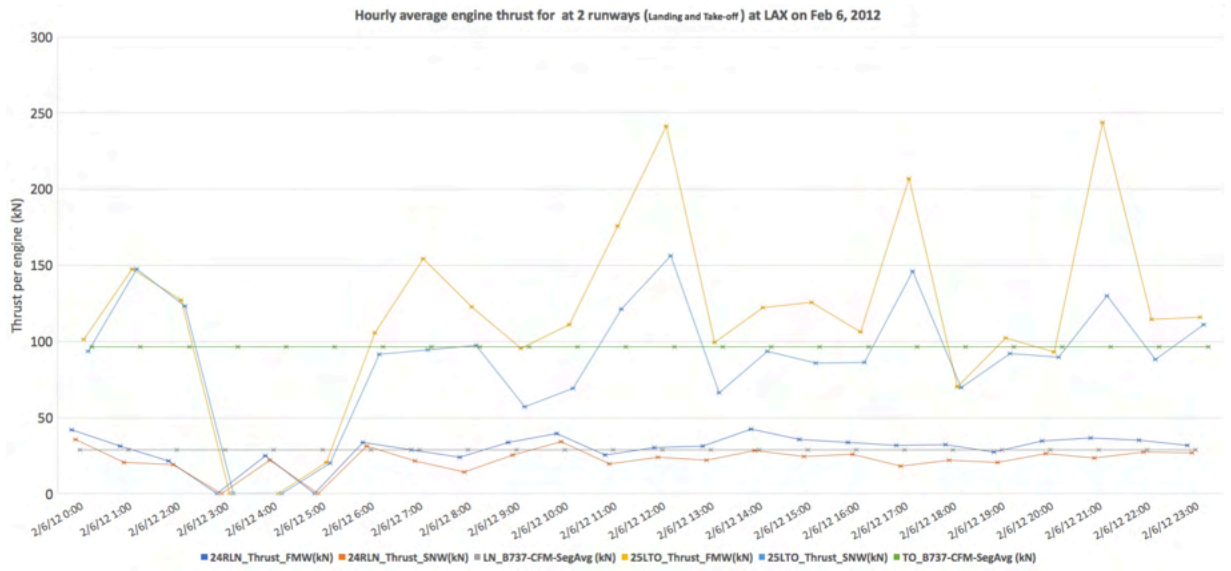

Figure A1. Comparison of hourly average thrust averaged by two methods: 1) fuel-burn-weighted (FBW) average thrust and 2) segment number average thrust (SNW) for 24R landing (24RLN) and 24L takeoff (24LTO) with the corresponding segment average thrust of the CFM engine of a Boeing 737-300 aircraft for landing (LN_B737-CFM-SegAvg(kn)) and takeoff (TO_B737-CFM- Seg Avg(kn)).

Table A2. Number of segments in the one-month AEDT file with and without zero-duration rows for February 2012 at LAX.

Type	Maximum altitude in data (ft)	No. of segments with zero-duration rows	No. of segments without zero-duration rows	Change in no. of segments when zero-duration rows are removed	% change in no. of segments when zero-duration rows are removed
All heights	13,865	269,2749	2,690,620	2,129	0.08
Used for ADM for 3000 ft	3,000	1,996,543	1,994,728	1,815	0.09

Table A3. Summary statistics of negative thrust segments and the altitude for negative thrust segments for one day in both winter (Feb. 1, 2012) and summer (July 1, 2012) AEDT data files.

	Winter 2012 file		Summer 2012 file	
Statistical parameters	Summary statistics of negative thrust (lb) segments	Summary statistics of altitude AFE (ft) of the negative thrust segments	Summary statistics of negative thrust (lb) segments	Summary statistics of altitude AFE (ft) of the negative thrust segments
Count	898	898	4983	4983
Mean	-201.68	2861.79	-315.22	4105.72
Standard deviation	238.23	534.89	209.35	1072.77
Minimum	-2740.30	-14.90	-1325.4	2582.00
25 Percentile	-322.37	2991.20	-444.32	2999.98
50 Percentile	-128.60	2991.20	-287.88	3873.98
75 Percentile	-74.60	3000.00	-140.74	5063.88
Maximum	-16.80	3000.00	-0.89	5999.98

Table A4. Comparison of AEDT-segment data for summer and winter 2012 files for LAX.

	Winter 2012 file	Summer 2012 file
AEDT-segment file		
Time duration	1.5 months (Feb. and Mar.)	2 months (July and Aug.)
File size		
Variables (columns)	38	126
No. of rows	3.7 million rows (3,661,723)	6 million (5,983,659)
Some new useful variables		Number of engines per aircraft, bypass ratio of the engine (will be used to calculate the air mass flow rate, propulsion efficiency, and exhaust speed to be used in the plume rise model)
Some new useful variables		Runway and gate number for both departure and arrival (will help to more easily extract direction-based emissions for each runway easier than the winter file)
AEDT-area (AERMOD file)		
Species files available	NO_x and SO_x	NO_x, SO_x, CO
# of sources	5,919	21,660

Table A5. Comparison of SO_x emissions between winter and summer AEDT-segment files for 2012 for LAX.

H	I	J	K	L	M
Data Period	**All height**	**Below 3000 ft (914.4 m)**	**Above 3000 ft (914.4 m)**	**Surface (height <= 0 ft)**	**Air (height 0-3000 ft)**
	SOx	**SOx**	**SOx**	**SOx**	**SOx**
	Total emission (surf+air) (g)	**Total emission (surf+air) (g)**	**Total emission (surf+air) (g)**	**Total emission (surface) (g)**	**Total emission (air) (g)**
Feb-12	26,525,852.59	17,423,672.72	9,102,179.87	8,107,894.32	9,315,778.40
Jul-12	20,239,295.90	13,685,934.80	6,553,361.09	7,129,882.36	6,556,052.48
Aug-12	19,766,199.69	13,332,544.60	6,433,655.09	6,883,357.60	6,449,187.00
July-Aug-12	40,005,495.62	27,018,479.44	12,987,016.17	14,013,239.96	13,005,239.48
	% OfTotalAllHeight	**% OfTotalAllHeight**	**% OfTotalAllHeight**	**% OfTotal-3000ft-Height**	**% OfTotal-3000ft-Height**
Feb-12	100	65.686	34.314	46.534	53.466
Jul-12	100	67.621	32.379	52.096	47.904
Aug-12	100	67.451	32.549	51.628	48.372
July-Aug-12	100	67.537	32.463	51.865	48.135
	Emission rate (ton/day)	**Emission rate (ton/day)**	**Emission rate (ton/day)**	**Emission rate (ton/day)**	**Emission rate (ton/day)**
Feb-12	**0.915**	**0.601**	**0.314**	**0.28**	**0.321**
Jul-12	**0.653**	**0.441**	**0.211**	**0.23**	**0.211**
Aug-12	**0.638**	**0.43**	**0.208**	**0.222**	**0.208**
July-Aug-12	**0.645**	**0.436**	**0.209**	**0.226**	**0.21**
Ref1: LAWA2013 Winter		**0.720**			
Ref1: LAWA2013 Summer		**0.716**			
Ref2: CSSI 2009	**1.004**				
	% Change of emission rate from Feb-2012	**% Change of emission rate from Feb-2012**	**% Change of emission rate from Feb-2012**	**% Change of emission rate from Feb-2012**	**% Change of emission rate from Feb-2012**
Jul-12	**-28.63387978**	**-26.62229617**	**-32.80254777**	-17.85714286	-34.26791277
Aug-12	**-30.27322404**	**-28.45257903**	**-33.75796178**	-20.71428571	-35.20249221
July-Aug-12	**-29.50819672**	**-27.45424293**	**-33.43949045**	-19.28571429	-34.57943925
LAWA 2013, Arunachalam, S. et al., 2013. LAX Air Quality and Source Apportionment Study Volume 1. Executive Summary. Los Angeles World Airports, Environ. Serv. Div. 2					
CSSI 2009 , JPDO – NextGen – TDM23: Investigation of Aviation Emissions for Future Aviation Activity Scenario. Washington DC					

Table A6. Comparison of NO_x emissions between winter and summer AEDT-segment files for 2012 for LAX.

H	I	J	K	L	M
Data Period	**All height**	**Below 3000 ft (914.4 m)**	**Above 3000 ft (914.4 m)**	**Surface (height <= 0 ft)**	**Air (height 0-3000 ft)**
	NOx	**NOx**	**NOx**	**NOx**	**NOx**
	Total emission (surf+air) (g)	**Total emission (surf+air) (g)**	**Total emission (surf+air) (g)**	**Total emission (surface) (g)**	**Total emission (air) (g)**
Feb-12	403,315,277.26	234,493,560.84	168,821,716.42	88,480,752.27	146,012,808.57
Jul-12	261,576,175.00	151,265,262.00	110,310,913.00	58,907,836.40	92,357,425.60
Aug-12	249,171,734.84	143,614,031.93	105,557,702.92	55,585,079.38	88,028,952.55
July-Aug-12	510,747,909.57	294,879,293.94	215,868,615.63	114,492,915.78	180,386,378.16
	% OfTotalAllHeight	**% OfTotalAllHeight**	**% OfTotalAllHeight**	**% OfTotal-3000ft-Height**	**% OfTotal-3000ft-Height**
Feb-12	100	58.142	41.858	37.733	62.267
Jul-12	100	57.828	42.172	38.943	61.057
Aug-12	100	57.637	42.363	38.704	61.296
July-Aug-12	100	57.735	42.265	38.827	61.173
	Emission rate (ton/day)	**Emission rate (ton/day)**	**Emission rate (ton/day)**	**Emission rate (ton/day)**	**Emission rate (ton/day)**
Feb-12	**13.907**	**8.086**	**5.821**	**3.051**	**5.035**
Jul-12	**8.438**	**4.88**	**3.558**	**1.9**	**2.979**
Aug-12	**8.038**	**4.633**	**3.405**	**1.793**	**2.84**
July-Aug-12	**8.238**	**4.756**	**3.482**	**1.847**	**2.909**
Ref: LAWA2013 Winter		**8.634**			
Ref: LAWA2013 Summer		**8.033**			
Ref2: CSSI 2009	**12.988**				
	% Change of emission rate from Feb-2012	**% Change of emission rate from Feb-2012**	**% Change of emission rate from Feb-2012**	**% Change of emission rate from Feb-2012**	**% Change of emission rate from Feb-2012**
Jul-12	**-39.32551952**	**-39.64877566**	**-38.8764817**	-37.72533596	-40.83416087
Aug-12	**-42.20176889**	**-42.70343804**	**-41.50489607**	-41.23238283	-43.59483615
July-Aug-12	**-40.76364421**	**-41.18229038**	**-40.1820993**	-39.46247132	-42.224429

LAWA 2013, Arunachalam, S. et al., 2013. LAX Air Quality and Source Apportionment Study Volume 1. Executive Summary. Los Angeles World Airports, Environ. Serv. Div. 2

CSSI 2009 , JPDO – NextGen – TDM23: Investigation of Aviation Emissions for Future Aviation Activity Scenario. Washington DC

Appendix B: Chemistry Modeling in Dispersion Models

a) 7 reaction mechanism (Azzi et al., 1992)

1	ROC + hv >[O2]> RP + ROC
2	RP + NO >[O2]> NO2
3	NO2 + hv >[O2]> NO + O3
4	NO + O3 > NO2
5	RP+RP > RP
6	RP+NO2 > SGN
7	RP+NO2 > SNGN

b) 12 reaction mechanism (Venkatram et al., 1997)

1	ROC1 + hv > RP +ROC1
2	AROM+hv > RP + AROM
3	TERP+hv > RP + TERP
4	RP + NO > NO2
5	NO2+hv > NO + O3
6	NO + O3 > NO2
7	RP + RP > RP + alfa*H2O2
8	RP + NO2 > RNO3
9	OH + SO2 > SO4
10	OH + NO2 > HNO3
11	OH + AROM > y1OC
12	OH + TERP > y2OC

Figure B1. Two reaction mechanisms for the chemistry module in the ADM dispersion model.

Table B1. Comparison of rate constants of Generic Reaction Set (GRS) mechanism (Azzi et al., 1992) with rate constants from two additional papers: (1) Valencia et al. (2018) and (2) Pournazeri et al. (2014).

No.	Reaction	Rate constant (ppm, min) Valencia et al. (2018)	Rate constant (ppm, min) Pournazeri et al. (2014)
1	ROC + hv > RP + ROC	k1=10000*exp(-4710/T) * k3 (min-1)	k1= 0:0067 k3 exp(-1000Gamma(1/T-1/316)) (min-1) where Gamma=4.7
2	RP + NO > NO_2	k2=5482 * exp(242/T) (ppm-1 min-1)	k2=3.58e6/T (ppm-1 min-1)
3	NO2 + hv > NO + O_3	k3=function of solar zenith angle (min-1)	k3= exp(-0.575/sin(theta)) where theta is the sun elevation angle (min-1)
4	NO + O_3 > NO_2	k4=2643 * exp(-1370/T) (ppm-1 min-1)	k4=9.24 *e5 (1/T)exp(-1450/T) (ppm-1 min-1)
5	RP + RP > RP	k5=10000 (ppm-1 min-1)	K5=10200
6	RP + NO_2 > SGN	k6=125 (ppm-1 min-1)	K6=120
7	RP + NO_2 > SNGN	k7=k6 (ppm-1 min-1)	K7=120

ROC: Reactive organic compounds
RP: Radical pool
SGN: Stable gaseous nitrogen products
SNGN: Stable nongaseous nitrogen products

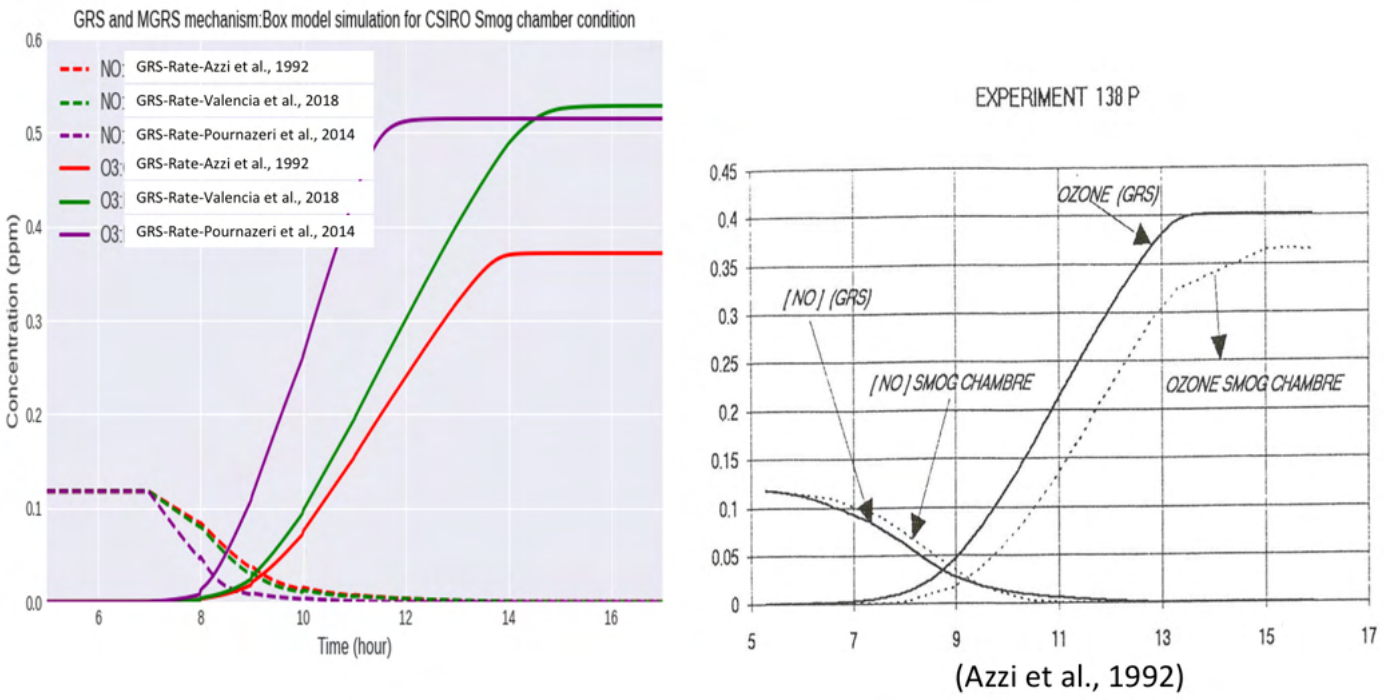

Figure B2. Left: A comparison of rate constants for the GRS mechanism (Azzi et al., 1992) with those from two additional papers (Valencia et al., 2018; Pournazeri et al., 2014). Right: A comparison with observations from Azzi et al. (1992) for the same conditions employed in the left figure.